University of Nebraska - Lincoln

DigitalCommons@University of Nebraska - Lincoln

Separating Touching Objects in Remote Sensing Imagery: The Restricted Growing Concept and Implementations

Leen-Kiat Soh
University of Nebraska, lsoh2@unl.edu

Costas Tsatsoulis
University of Kansas, tsatsoul@eecs.ukans.edu

Different simulations allow us to asses the existence of some situations in which the use of ICE-COR is of interest.

Unfortunately, we have no theoretical result to present concerning the asymptotic behavior of ICE-COR. We hope to devote to this important subject some efforts in our future works.

REFERENCES

[1] J. Besag, "On the statistical analysis of dirty pictures," *J. R. Statist. Soc. B*, vol. 48, pp. 259–302, 1986.

[2] J. M. Boucher and P. Lena, "Unsupervised Bayesian classification, application to the forest of Paimpont (Brittany)," *Photo Interp.*, vol. 32, no. 1994/4, 1995/1-2, pp. 79–81, 1995.

[3] H. Caillol, W. Pieczynski, and A. Hillon, "Estimation of fuzzy Gaussian mixture and unsupervised statistical image segmentation," *IEEE Trans. Image Processing*, vol. 6, no. 3, pp. 425–440, 1997.

[4] R. Chellapa and A. Jain, *Markov Random Fields, Theory and Application*, A. Jain, Ed. San Diego, CA: Academic, 1993.

[5] Y. Delignon, A. Marzouki, and W. Pieczynski, "Estimation of generalized mixture and its application in image segmentation," *IEEE Trans. Image Processing*, vol. 6, pp. 1364–1375, Oct. 1997.

[6] M. M. Dempster, N. M. Laird, and D. B. Rubin, "Maximum likelihood from incomplete data via the EM algorithm," *J. R. Stat. Soc. B*, vol. 39, pp. 1–38, 1977.

[7] S. Geman and G. Geman, "Stochastic relaxation, Gibbs distributions and the Bayesian restoration of images," *IEEE Trans. Pattern Anal. Machine Intell.*, vol. PAMI-6, pp. 721–741, June 1984.

[8] N. Giordana and W. Pieczynski, "Estimation of generalized multisensor hidden Markov chains and unsupervised image segmentation," *IEEE Trans. Pattern Anal. Machine Intell.*, vol. 19, no. 5, pp. 465–475, 1997.

[9] Z. Kato, J. Zerubia, and M. Berthod, "Unsupervised parallel image classification using Markovian models," *Pattern Recognit.*, vol. 32, pp. 591–604, 1999.

[10] S. Lakshmanan and H. Derin, "Simultaneous parameter estimation and segmentation of Gibbs random fields," *IEEE Trans. Pattern Anal. Machine Intell.*, vol. 11, pp. 799–813, 1989.

[11] J. Marroquin, S. Mitter, and T. Poggio, "Probabilistic solution of ill-posed problems in computational vision," *J. Amer. Statist. Assoc.*, vol. 82, pp. 76–89, 1987.

[12] W. Pieczynski, "Statistical image segmentation," *Mach. Graph. Vis.*, vol. 1, no. 1/2, pp. 261–268, 1992.

[13] W. Pieczynski, J. Bouvrais, and C. Michel, "Unsupervised Bayesian fusion of correlated sensors," in *1st Int. Conf. Multisource–Multisensor Information Fusion*, Las Vegas, NV, July 6–9, 1998.

[14] W. Qian and D. M. Titterington, "Stochastic relaxations and EM algorithms for Markov random fields," *J. Statist. Comput. Simulat.*, vol. 40, pp. 55–69, 1992.

[15] L. R. Rabiner, "A tutorial on hidden Markov models and selected applications in speech recognition," *Proc. IEEE*, vol. 77, no. 2, pp. 257–286, 1989.

[16] R. A. Redner and H. F. Walker, "Mixture densities, maximum likelihood and the EM algorithm," *SIAM Rev.*, vol. 26, pp. 195–239, 1984.

[17] D. M. Titterington, A. F. M. Smith, and U. E. Makov, *Statistical Analysis of Finite Mixture Distribution*. New York: Wiley, 1985.

[18] L. Younes, "Parametric inference for imperfectly observed Gibbsian fields," *Prob. Theor. Relat. Fields*, vol. 82, pp. 625–645, 1989.

Separating Touching Objects in Remote Sensing Imagery: The Restricted Growing Concept and Implementations

Leen-Kiat Soh and Costas Tsatsoulis

Abstract—This paper defines the restricted growing concept (RGC) for object separation and provides an algorithmic analysis of its implementations. Our concept decomposes the problem of object separation into two stages. First, separation is achieved by shrinking the objects to their cores while keeping track of their originals as masks. Then the core is grown within the masks obeying the guidelines of a restricted growing algorithm. In this paper, we apply RGC to the remote sensing domain, particularly the synthetic aperture radar (SAR) sea ice images.

Index Terms—Morphology, object separation, remote sensing imagery, restricted growing.

I. INTRODUCTION

When two gray level objects touch with shared boundaries, it makes shape analysis and recognition difficult in areas such as industrial vision applications [3], in aerial image and terrain analysis [7] or in shape analysis [5]. The objectives of our work are to achieve object separation, and to preserve (or approximate as closely as possible) the object's original shape and size. The tradeoff between separation and preservation of size and shape is inherent in all object separation algorithms. To address this problem, we have designed a technique based on the restricted growing concept (RGC), that achieves separation and, then, reestablishes the sizes and shapes of the objects lost or distorted during the separation process by performing restricted growing.

In this paper, we present the restricted growing concept and address the issues of preserving details through different designs of masks, investigate the use of morphological reconstruction h-domes in extracting cores, compare the differences between the performance of the morphological operators in synthetic and remotely sensed images, and describe a reverse skeletonization algorithm to guide the growth of object pixels in the image. We finally present twelve algorithms of RGC and examine their weaknesses and strengths when applied to synthetic aperture radar (SAR) sea ice images.

II. RESTRICTED GROWING CONCEPT

The main idea behind the RGC is to decompose the object separation problem into two steps: The first step achieves separation, accomplished by *shrinking* objects such that each object is separated from its touching neighbors. The second step preserves size and shapes by growing the shrunk objects to restore them. To ensure that the separation established after the first stage is not disturbed, our growing process is *restricted*.

In our approach, a *mask object* is a version of the original object such that the original size of the object is preserved. Mask objects are usually interconnected and can encompass one or more core objects. An image with mask objects is a *mask image*. A *core object* is a version of the original object such that its linkages to neighboring objects are disconnected, satisfying object separation. Such an object is reduced in

size, but it captures the general shape of its original version. An image with core objects is a *core image*. Finally, a *restricted growing algorithm* grows a core object within the boundary of its corresponding mask object while preserving the object's separation from its neighbors. This definition implies that the growing process stops either when the boundary of the object has been reached or when further growing will damage the object's separation from its neighbors. Thus, conventional region growing [12] or morphological dilation schemes are not restricted growing algorithms.

A. Generating the Mask Image

Our implementation basis for the mask image is gray level global thresholding. We use threshold slices, S_t, obtained by thresholding the image at intensity t, as the changing environment on which we base the assessment of the confidence that a pixel belongs to an object. The set of environments or threshold slices is $\Omega(T, I, N)$, where T is the starting threshold, I the interval between successive slices, and N the number of slices: $\Omega_{\mathrm{mask}} = \Omega(t(i, j), 2, 3) = \{S_{t(i, j)}, S_{t(i, j)+2}, S_{t(i, j)+4}\}$, where $t(i, j)$ is the threshold computed at pixel (i, j) during the segmentation process, $I_{\mathrm{mask}} = 2$, and $N_{\mathrm{mask}} = 3$. To obtain the accumulated confidence $c_{S_t}(i, j)$ of a pixel being an object at S_t, we compute the ratio of the pixel's neighbors that have survived the slicing of S_t, and then set $C_{\mathrm{mask}}(i, j) = \sum_{S_t \in \Omega_{\mathrm{mask}}} c_{S_t}(i, j)$. Finally, to label each pixel in the mask image, we compare $C_{\mathrm{mask}}(i, j)$ to a prespecified threshold, T_{mask}; if the $C_{\mathrm{mask}}(i, j)$ of a pixel at (i, j) is greater than or equal to T_{mask}, then that pixel is an object pixel in the mask image. T_{mask} has been experimentally determined as 0.75 for synthetic aperture radar (SAR) sea ice images. Note that the above algorithm has three important parameters, i.e., T_{mask}, I_{mask}, and N_{mask}, that system designers can adjust to accommodate their specific needs and domains of applications during the development phase of their object separation software. Please refer to [9] for a detailed description of the experiments.

B. Generating the Core Image

We investigated two techniques to generate core objects. The first used morphological reconstruction [10] which extracts as core objects h-domes of regions in an image. First, h is subtracted from the original image for all pixels to obtain the minus-h image. Second, the features in the minus-h image are reconstructed to obtain regional maxima. Third, the reconstructed minus-h image is subtracted from the original image and the leftover features are the h-domes. We adapted this technique to be restricted by the mask image to preserve separation. We found through experiments that even though reconstruction and h-domes can be applied successfully to well-behaved or synthetic images, they are not suitable for remotely-sensed imagery such as SAR sea ice images due to inherent speckle noise. The noise effects and intrinsic heterogeneity within sea ice regions forbid the reconstruction from forming good quality plateaus, resulting in many trivial cores. Thus, to obtain core object pixels, we used $\Omega_{\mathrm{core}} = \Omega(t(i, j), 2, 5)$, where $I_{\mathrm{core}} = 2$, and $N_{\mathrm{core}} = 5$, and $C_{\mathrm{core}}(i, j) = \sum_{S_t \in \Omega_{\mathrm{core}}} c_{S_t}(i, j)$. Similar to T_{mask}, a threshold value T_{core} has been experimentally determined to be 0.50 for SAR sea ice images. Our core extraction step was determined to be able to separate touching objects with up to 25 shared boundary pixels and obtain primary cores in up to 15% noise-corrupted images [9].

C. Restricted Growing Algorithm Using Reversed Skeletonization

Our restricted growing algorithm uses reverse skeletonization to grow core objects within the boundary of their corresponding mask objects while preserving existing separation among the core objects.

As the basis for reverse skeletonization we used the skeletonization algorithm described in [11]. Our restricted growing algorithm was based closely on the thinning algorithm, with the following tests and conditions.

Test 1—Potential Growing Condition: If a pixel in the core image is a nonobject pixel and its corresponding pixel in the mask image is an object pixel, then the pixel is qualified for a further test.

This test selects only nonobject core pixels for potential growth, guaranteeing that we only grow core objects within the boundary of mask objects. In addition, pixels that are nonobject in both core and mask images are deemed as true nonobject and rejected from growing.

Test 2—Isolation Condition: If the pixel in the core image does not have an object pixel in its core image as an 8-neighbor, then the pixel is disqualified.

This condition avoids erroneous separation within an object. For example, small dark specks in an object would be eroded to nonobject pixels during the generation of the core image.

Test 3—Connectivity Condition 1: If the pixel in the core image has seven or eight object pixels in its core image 8-neighborhood, then the pixel is grown.

If the 8-neighborhood of a pixel has seven or more object pixels, that means all object pixels in that neighborhood are connected. Hence, the growth of the pixel from nonobject to object does not damage the existing (or nonexisting) separation.

Test 4—Connectivity Condition 2: If the pixel in the core image has no or one 1-0 transition in its core image 8-neighborhood, then the pixel is grown.

If no or one 1-0 transition is found, that means all object pixels in the area are connected and thus a growth is safe. This condition is analogous to the second condition of the original skeletonization algorithm. Note that Tests 3 and 4 could be combined to streamline the design.

Test 5—Connectivity Condition 3: If the 8-neighborhood of the pixel in the core image matches one of the four corner patterns, then the pixel is grown.

The *corner patterns* are shown in Fig. 1. Each of these patterns could have two or more 1-0 transitions yet have all its object pixels connected and thus has no separation to preserve. This test combines the last two conditions of the thinning algorithm. Note that the last two conditions cover all relevant 8-neighborhood patterns: Test 4 covers all cases with fewer than two 1-0 transitions; Test 5 covers the rest.

III. ANALYSIS OF DIFFERENT IMPLEMENTATIONS OF RGC

The algorithm of the basic RGC can be expressed in the following pseudo code:

```
RGC
(1) Generate the mask image.
(2) Generate the core image.
(3) Scan the core image in some manner,
and for each pixel encountered:
(a) Apply the tests (as described in Sec-
tion  II.C).
(b) If the pixel passes the tests, Then
convert it to an object pixel.
(c) If no change, Then move on to the next
pixel.
(4) Repeat step (3) Until the core image
converges.
```

The two keys to the design of the algorithm are how one scans the image and how one selects the next pixel for processing. Here we discuss twelve different algorithms:
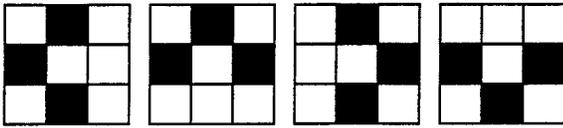
Fig. 1.   Patterns examined in Test 5: Dark pixels are object pixels; unshaded pixels are "don't care" pixels.

RGC_BASIC uses raster scanning, from top to bottom, left to right. After each growth, the raster simply moves to the next column and row to reduce horizontal (or vertical) growth tendency in the image. In RGC_JUMP, the scanning process jumps to a pixel JUMP_STEP away to prevent the growth of the current pixel from affecting the next pixel immediately. RGC_BCOLOR uses blob-coloring to grow pixels more aggressively; when two locally separated object neighbors are parts of a connected object, a growth is permissible. Hence, if all tests fail to grow the pixel yet all object neighbors of the pixel share the same blob-color, then we grow the pixel. RGC_BCOLOR_JUMP combines RGC_JUMP and RGC_BCOLOR. RGC_DIST utilizes the 8-distance transform to record the shortest distance of an object pixel from a nonobject pixel [8]. This grows each ring of a region at a time for all regions from the innermost pixels outward. RGC_DIST_BCOLOR combines 8-distance transform and blob coloring. In morphology, a two-scan iteration is often used to obtain balanced consideration for all pixels in the image in both directions. Thus, we implemented six more similar algorithms but with two-scans.

We performed a number of experiments to test the algorithms on various SAR sea ice images. The results were visually evaluated for quality of separation, shape and size preservation. The following conclusions were drawn:

1) The two-scan iteration design offers better balance in regional growth, compared to the one-scan design; the regions are less complicated and more fully grown.

2) Implementations that include jumps to avoid immediate growth effects fare better in terms of shape definition. However, jumps also introduce breaks in the regions, and algorithms without jumps establish fuller regions by absorbing more pixels from neighboring ones.

3) By utilizing blob coloring in the restricted growing algorithm we obtain regions that close better and are more compact. "Hairline" effects that are sometimes evident because of breaks within regions are reduced. However, with blob coloring, nonobject pixels are more sporadic and less connected. Thus, we recommend an implementation without blob coloring when nonobject breaks are important.

4) The implementations with distance transform do not perform as well as those without. There are two possible reasons. First, SAR sea ice images are noisy and the distance transform creates holes in a region. These holes could be seen as lakes and thus the topology of the region in terms of the shortest distance to a nonobject pixel is no longer in a uniform ring radiating outward from the center of the region, retaining noise effects. Second, the 8-distance transform does not represent the actual distance between pixels—the diagonal neighbors are further from the center than the direct-neighbors.

5) Because of the inherent noise of SAR sea ice images, we do not recommend using distance transform alone because it dominates the growth patterns and retains noise effects. Combining the distance transform with blob coloring or two-scan iteration improves the results. Further, we do not recommend using two-scan iteration, blob coloring, and jumps together, since the design extracts blocky regions.

6) In general, most of the twelve algorithms yield good object separation results. They tolerate speckle noise in object separation and reduce noise effects in object definition. Our evaluation of the results indicates that the algorithm RGC_BCOLOR is the most consistent, due to the one-scan design and the ability of the blob coloring-based approach to absorb negligible noise effects.

Note that we do not provide a resolution or recommend a size or shape of a "hole" that our RGC algorithms might fail to absorb. If one chooses to implement restricted growing using a 5×5 neighborhood, or a 4-neighhorhood, or other neighborhoods, the resulting constraints will differ significantly. Also, we assume that tiny holes are noise-induced and should be absorbed, as explained in Test 2. On the other hand, large, well-defined holes should be retained and should not get filled by neighboring object pixels.

In terms of performance, algorithms that implement blob coloring perform faster; those using distance transform perform more slowly; and finally those with jumps even more slowly. This is because of the skipping of pixels per iteration, due to either distance transforms or jumps, and the consequent additional number of iterations needed to converge the core image. On an SGI Challenge L/6, with 256 Mb RAM, execution times on a 450×600 image averaged between 9 s for the fastest algorithms to approximately 6 min for the slowest ones.

IV. COMPARISONS TO OTHER WORK

Banfield and Raftery [1] used a method called erosion-propagation (EP) algorithm coupled with clustering about principal curves [4] to identify objects in satellite images. This object separation technique suffers from several disadvantages:

1) number of iterations required to achieve separation has to be determined manually for each image;

2) objects smaller than $(2i + 1) \times (2i + 1)$ pixels, where i is the number of iterations, will be eliminated;

3) objects do not preserve their original size.

In another approach [2], a tagging algorithm was used to separate objects with weak connections. However, this technique separated only regions connected by corners or by one-pixel bridges, rendering it incapable of achieving separation when stronger connections occur. Noordmans and Smeulders [6] proposed a strategy that detects and characterizes isolated and overlapping spots in images where spots are defined as image details without inner structure. To apply the strategy to our domain, one would have to define a substantial, nontrivial set of spot models, including expanding the suggested models' parameters to involve both Cartesian axes and the intensity axis, which would result in inefficient modeling and its subsequent matching.

V. CONCLUSIONS

The RGC algorithms presented here do not restore "high frequent" details such as a 20-point star or a fine-toothed circle. Instead, our algorithms have been designed to analyze unstructured objects (with irregular shapes and sizes) in remotely sensed images and natural scenes and not man-made objects.

REFERENCES

[1] J. Banfield and A. E. Raftery, "Ice floe identification in satellite images using mathematical morphology and clustering about principal curves," *JASA*, vol. 87, no. 417, pp. 7–16, 1992.

[2] J. Daida, R. Samadani, and J. F. Vesecky, "Object-oriented feature-tracking algorithms for SAR images of the marginal ice zone," *IEEE Trans. Geosci. Remote Sensing*, vol. 28, no. 4, pp. 573–589, 1990.

[3] R. C. Gonzalez, "Industrial computer vision," in *Advances in Information Systems Science*, J. T. Tou, Ed.   New York: Plenum, 1985, pp. 345–385.

[4] T. Hastie and W. X. Stuetzle, "Principal curves," *JASA*, vol. 84, pp. 502–516, 1989.

[5] D. Haverkamp, L.-K. Soh, and C. Tsatsoulis, "A comprehensive, automated approach to determining sea ice thickness from SAR data," *IEEE Trans. Geosci. Remote Sensing*, vol. 33, no. 1, pp. 46–57, 1995.

[6] H. J. Noordmans and A. W. M. Smeulders, "Detection and characterization of isolated and overlapping spots," *Comput., Vis., Image Understand.*, vol. 70, no. 1, pp. 23–35, 1998.

[7] L. O'Gorman, "$k \times k$ thinning," *Comput., Vis., Graph. Image Process.*, vol. 51, no. 2, pp. 195–215, 1990.

[8] D. A. Rothrock and A. S. Thorndike, "Measuring the sea ice floe size distribution," *J. Geo. Res.*, vol. 89, no. C4, pp. 6477–6486, 1984.

[9] L.-K. Soh and C. Tsatsoulis, "The restricted growing concept for object separation," University of Kansas, Lawrence, KS, ITTC-FY98-TR-11 810-02, ITTC, 1998.

[10] L. Vincent, "Morphological grayscale reconstruction in image analysis: Applications and efficient algorithms," *IEEE Trans. Image Processing*, vol. 2, no. 2, pp. 176–201, 1993.

[11] T. Y. Zhang and C. Y. Suen, "A fast parallel algorithm for thinning digital patterns," *Commun. ACM*, vol. 27, no. 3, pp. 236–239, 1984.

[12] S. W. Zucker, "Region growing: Childhood and adolescence," *Comput., Graph., Image Process.*, vol. 5, pp. 382–399, 1976.